UNDERSTANDING BEAM LOSSES IN HIGH-INTENSITY PROTON ACCUMULATOR RINGS*

Robert J. Macek# and Jeffrey S. Kolski, LANL, Los Alamos, NM 87545, USA

Abstract

Beam losses and the resulting radio-activation of accelerator components are major considerations governing the operations and performance of medium-energy, high-intensity proton accumulator rings using H- charge exchange injection such as the Los Alamos Proton Storage Ring (PSR). Several beam loss mechanisms contribute including beam scattering (nuclear and large angle Coulomb scattering) in the injection foil, production of excited states of H0 in the H- injection stripper foil that subsequently field strip in the magnetic fields down stream of the foil, halo growth from space charge effects, beam instabilities and losses from the fast extraction process. These are now well understood based on the progress in the diagnosis, measurement, and modeling of beam losses at PSR and related rings. The roles of the computer codes MAD8 [1], ORBIT [2], G4Beamline [3], and others used in modeling beam losses are discussed, and the modeling results are compared with relevant experimental data.

INTRODUCTION

Minimizing uncontrolled beam losses is one of the most important objectives in the design, operations and development of high-intensity proton accumulator rings that use many hundreds to thousands of turns of H- charge exchange injection such as the Los Alamos Proton Storage Ring (PSR) or the accumulator ring for the Spallation Neutron Source (SSN) at the Oak Ridge National Laboratory. Similar concerns hold for the rapid cycling synchrotrons at the heart of the spallation neutron sources at the Rutherford Appleton Laboratory in the UK and the Japan Proton Accelerator Complex (J-PARC). To limit radio-activation of accelerator components in order to permit hands-on maintenance, it has become a rule-of-thumb to limit uncontrolled beam losses to the 1 Watt/meter level.

The Los Alamos PSR was a pioneering effort in the use of charge exchange injection for a full power, high intensity accumulator ring to drive a short pulse spallation neutron source [4]. Much has been learned about beam losses in this ring since first beam in 1985. Until 1998, PSR used a two-step injection process i.e., stripping of H- to H0 in a high field dipole then stripping to H+ in a stripper foil. By 1993 the beam losses for the two-step injection were reasonably well understood and had been reduced significantly by a number of improvements [5]. It should also be noted that by 1993, it was shown that the 0.2-0.3% fractional losses on the first turn were explained by the production and stripping of H0(n=3, and 4) excited states produced in the stripper foil that subsequently Lorentz strip in the first dipole down stream of the injection foil [6].

In 1998, the upgrade of PSR to direct (one step) H- injection was completed [7] and resulted in a factor of ~3 reduction in the fractional beam losses. PSR has since then operated at 100-125 μA with total fractional uncontrolled losses of 0.2% - 0.3%.

PSR LAYOUT

A layout of PSR after the 1998 upgrade is shown in Figure 1. It is a small ring of 90.2 m circumference with 10 sections and FODO lattice. In normal operations, 800 MeV beam is accumulated for ~1750 turns to provide 100-120 μA (5-6 μC/pulse) at 20 Hz for the main user, the LANSCE spallation neutron source at the Lujan Center. The "waste" beam i.e., H- that did not strip and H0 is transported via a large aperture beam line to a graphite beam dump capable of handling 10 μA or 8 kW of beam power. Single turn extraction is accomplished with two strip line kickers and a septum magnet system. It is worth noting that in high peak intensity beam studies, as much as 10 μC was successfully accumulated in 3400 turns.

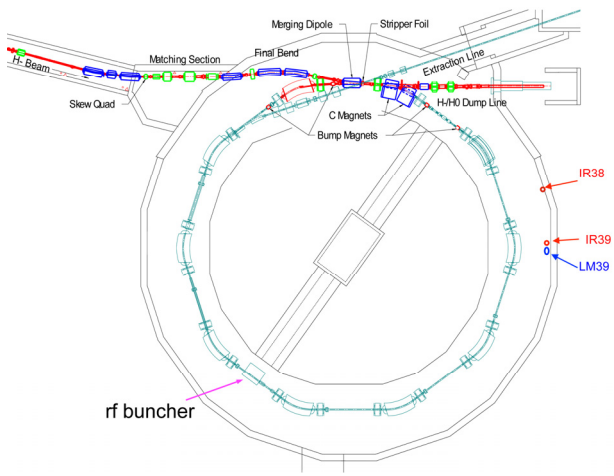

Figure 1: PSR layout since 1998.

The injection stripper foil is a ribbon 12 mm wide by 40 some mm long made up of two 200 microgram/cm^2 layers. Today, each layer is a hybrid composite of carbon and boron in a method developed by Professor Sugai at KEK for enhancing foil lifetime [8]. Numerous 4 micron carbon fibers are stretched across the frame to keep the foil from moving.

The stripper foil is offset from the final H+ closed orbit, and the H- beam strikes the foil on a corner. A

*Work supported by US DOE under contract DE-AC52-06NA25396.
#macek@lanl.gov

ISBN 978-3-95450-173-1

programmed closed orbit bump in the vertical is used for phase space painting as shown in the diagrams of Figure 2. The objective is to minimize the number of foil hits by the stored beam and minimize the space charge density of the beam.

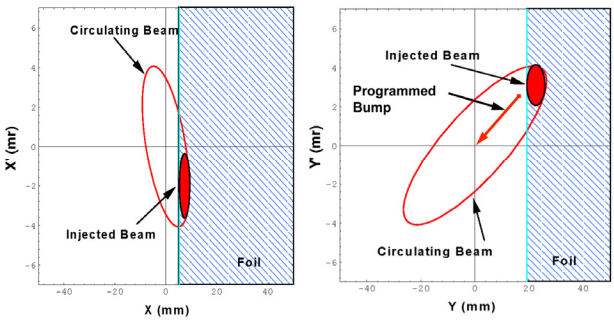

Figure 2: Injection phase space painting at the stripper foil location.

PSR BEAM LOSS MONITORING

Total beams losses are measured by the sum of the average current from 19 ion chambers (**IR**) located on tunnel wall opposite each dipole and halfway in between. These locations for IR38 and IR39 are illustrated in Figure 1. This pattern is repeated for each section of ring. The IR sum is calibrated by injecting up to 0.4 μC and letting it all be lost with no extraction. We check the uniformity (15-30%) of the system response by spilling locally using various closed orbit bumps. A newer method to calibrate and check uniformity of response is described at the end of this section.

A fast response loss monitoring system (~10 ns) consists of 10 scintillation detectors (**LM**) located opposite each dipole and next to the IRn9's. The location for LM39 is also shown in Figure 1. Again, the pattern is repeated for each section of the ring.

Typical beam losses and activation data are shown on a control room loss monitor display in Figure 3. The activation measurements added in color to the display were taken from a 2008 survey ~1 day after the beam was turned off for a regular maintenance period. The beta-gamma activation readings are taken 30 cm from the beam pipe. The graphic shows a typical beam for operations of ~110 μA with a typical beam loss ~0.0025 (0.28 μA, 225W). Losses were measured from the sum of Ion Chamber (IR) readings and a calibration constant.

The high loss regions and high activation regions are located in the injection section plus the following section as well as the extraction region. The graphic in Figure 4 shows that activation has a reasonable correlation with the loss monitor data.

A new method of IR "calibration" and uniformity checks was carried out in 2012. The previous method used a known low-intensity coasting beam that was not extracted, hence was lost entirely. This assured that that the amount of lost beam was well determined. Our concern was that even with various local bumps the losses appeared mostly in just a few spots. The new method used a standard bunched beam accumulation and a short store (100 μs) plus extraction but used large bumps (35-45 mm) in order to lose a large fraction (50% or more) of the beam. In this way the amount of beam lost could be well determined with current monitors in the ring. We used a low intensity beam of ≤ 0.4 μA average current in order to limit activation of ring during the large fractional loss measurements.

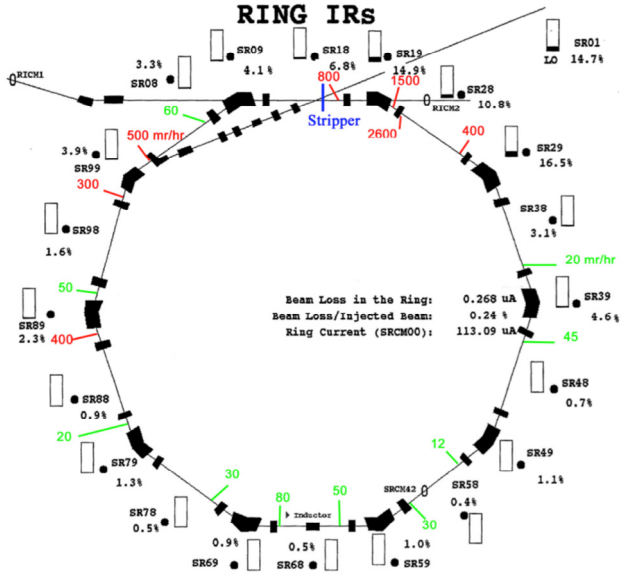

Figure 3: Control room display of beam losses with activation map added. Each IR is % of full scale.

An ORBIT simulation with large bumps showed most of the beam was lost in one quadrupole at the bump location. Thus, losses were more localized at calculated bump locations and avoided the uncertainty of loss locations and shielding effects during the long store of the coasting beam method. For each large bump, a calibration number (equal to the sum of all 19 IR values divided by the current lost) was obtained. Figure 4 is a plot of the "calibration" value for the bumps used in each section of the ring in the 2012 study.

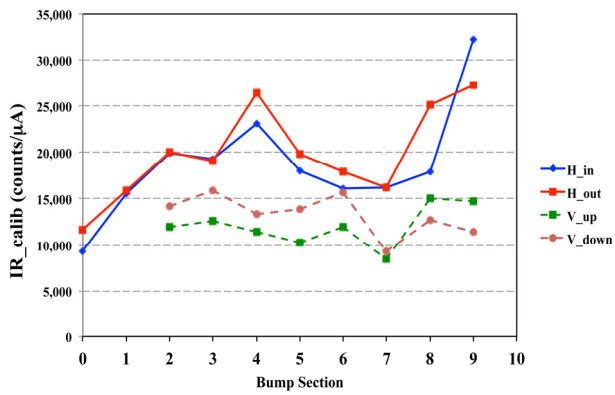

Figure 4: Plot of IR_calibration values for the various bumps in the 2012 study.

ISBN 978-3-95450-173-1

BEAM LOSS MECHANISMS

Several significant loss mechanisms for PSR have been identified and studied extensively. These include:

1. Foil scattering, which includes:
   a. Nuclear elastic and inelastic scattering.
   b. Rutherford scattering, which we designate as "large angle Coulomb scattering"
2. Excited states of H0(n) (n>2) produced from H- in the stripper foil that subsequently Lorentz strip in the first dipole down stream of the foil.
3. Extraction losses during the single turn extraction process at the end of accumulation.
4. Betatron resonance crossing, which can be avoided by a suitable operating point.
5. Beam instabilities, in particular, the two-stream e-p instability [9,10] which is generally avoided for production beams by sufficient rf buncher voltage.
6. Space charge emittance growth, which is not very significant for routine production beam intensities less than 6 μC/macropulse.

Items 1., 2., and 3., above are important for routine production beams and are discussed more fully in the following sections. In general, each of these was studied both experimentally and by various modeling methods.

Foil Scattering

The major component of losses (60-75% of total loss) is from foil scattering i.e., nuclear elastic and inelastic scattering plus large angle Coulomb scattering (larger than the angles given by the limiting apertures in the ring. Cross-sections for these are well known, but we need to know the number of foil hits by the accumulated beam, which are typically 100-150 for the average proton, and which we obtain from simulations and/or from calibrated foil current measurements.

We can measure the current from the foil, which is primarily from secondary emission from beam hitting the foil. The graph in Figure 5 shows signals from 1/17/03 production at 115 μA and demonstrates that the beam loss signal tracks the foil current. By knowing the secondary emission yield (SEY) we can get the number of foil hits per stored proton from the foil current signal. For an SEY of 1.06% for carbon foils (measured 6/13/02), the foil signal implies 70 foil hits per average proton in the beam. We measure SEY at low intensity by running the foil for nearly on axis injection so that all protons hit the foil every turn. This has not been done for about a decade so the simulation probably gives a more reliable foil hit number for contemporary foils.

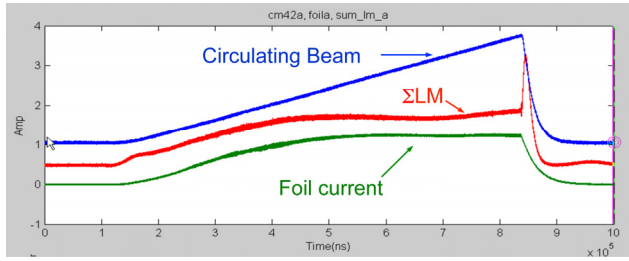

Figure 5: Signals from 1/17/03 production, foil current (green), LM sum (red), circulating beam current (blue).

For a simple estimate of losses from **nuclear interactions** including elastic and quasi-elastic scattering, we use published data (from PDG handbook) on nuclear collision lengths for carbon i.e., $\lambda_T = 59.2$ g cm^{-2}, thus the fractional loss from 150 foil traversals is 0.00102.

For **large angle Coulomb scattering** we use a simple model of an on-axis, pencil beam hitting the foil with limiting acceptance angles, θ_{xl} or θ_{yl} , obtained from limiting apertures, X_A and Y_A given by:

$$\theta_{xl}^2 = \frac{X_A^2}{\beta_{fx}\beta_{xA}} \quad \text{and} \quad \theta_{yl}^2 = \frac{Y_A^2}{\beta_{fy}\beta_{yA}}$$

For typical PSR production beam parameters, $\theta_{xl} = 7$ mr, $\theta_{yl} = 3.3$ mr. Next, we integrate the Rutherford scattering differential cross-section in the small angle approximation (form Jackson, "Electrodynamics, equation 13.92 [11]) over the region outside the ring acceptance from $|\theta x| = \theta x1$ to ∞ and $|\theta y| = \theta yl$ and obtain the cross-section σ_{lost} for lost protons:

$$\sigma_{lost} = C_0\left[\frac{1}{\theta_{xl}\theta_{yl}} + \frac{1}{\theta_{xl}^2}\tan^{-1}\left(\frac{\theta_{yl}}{\theta_{xl}}\right) + \frac{1}{\theta_{yl}^2}\tan^{-1}\left(\frac{\theta_{xl}}{\theta_{yl}}\right)\right]$$

The probability (per foil traversal) of a single large angle scattering that leads to particle loss is $P=N\sigma_{lost}t$ where N is the number of atoms per unit volume and t the foil thickness. Using PSR parameters and a 400 μg/cm^2 carbon, $P = 6.1\text{x}10^{-6}$ per foil traversal, or for a typical150 foil hits/proton, the fractional loss from large angle Coulomb scattering is 0.00091.

Thus, the fractional loss from foil scattering = sum losses from large angle Coulomb loss + the loss from nuclear scattering = 0.0019 (for 150 foil traversals per proton) as estimated by the simple model models above. This compares favourably with typical measured total fractional loss of ~0.0025.

Excited States of H0(n) (n>2)

A small faction (~$5\text{x}10^{-4}$) of the H- atoms hitting the stripper foil emerge as excited states of H0 [6,12], which can subsequently be field stripped part way into the first dipole downstream of the foil and fall outside of the acceptance of the ring and are lost. A horizontal phase space diagram to illustrate this is shown in Figure 6 for a particular n=4 Stark state (n1=3, n2=0, m=0 for the remaining parabolic quantum numbers).

ISBN 978-3-95450-173-1

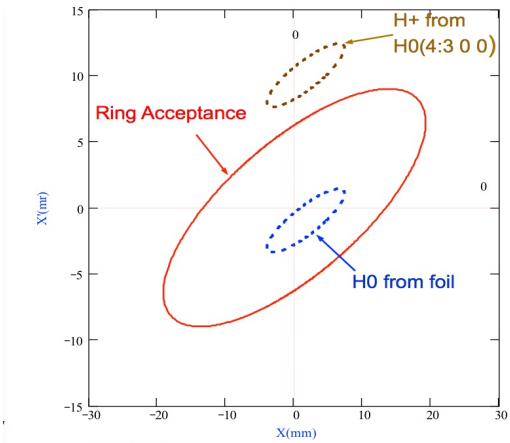

Figure 6: Horizontal phase space diagram depicting beam loss from an excited Stark state H0(4:3 0 0).

The various phase ellipses are projected to the entrance of first dipole (SRBM11) downstream of the stripper foil. The H+ from the H0(4: 3 0 0) state is bent by ~11 mr less than protons from the foil and thus falls outside of the acceptance of the ring and is lost.

To obtain the angle deficit, theta, for this stripped Stark state, we use formulas from Damburg and Kolosov [13] for the line width of Stark states and obtain the stripping probability as a function of magnetic field. From these and the magnetic field as a function of distance into the magnet we can obtain the probability distribution for theta (units of mr). From similar calculations for other Stark states, we find that n=1 and 2 states are not stripped in the first dipole while all of n=3, n=4 and n=5 Stark states are stripped and most are lost. Higher Stark states strip easily and contribute to beam halo in the ring acceptance.

Total losses during accumulation can also be monitored by a fast response system (~10 ns) of 10 scintillation detectors (LM) opposite each ring dipole. The fast response of the LMsum signal is useful for measuring losses from excited states, which would cease at the end of accumulation and show a step drop in the signal if the beam is stored for a 100 μs or so. When these were first observed in the early days of PSR, the step drop was designated "1st turn losses". An example of such signals from an experiment 6/11/2002 is shown in Figure 7, where a typical 4-layer carbon foils (~400 μg/cm^2) of that era was used. Total fractional losses during accumulation were ~ 0.0047, and the data indicates "excited state losses" of 44% of the total losses. Data for an HBC 2-layer foil in 2010 showed 18% of the total loss was from excited states.

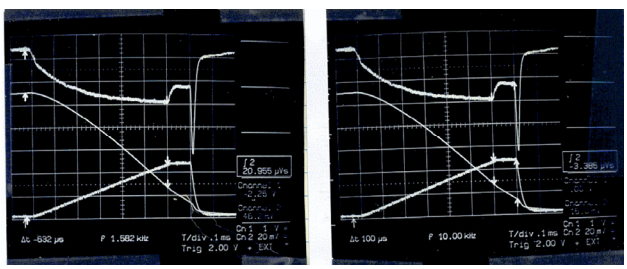

Figure 7: Measurement of 1st turn loss 6/11/2002. Top curves LMsum signal, center integral of LMsum, bottom CM42 current monitor.

Extraction Losses

These are measured by special fast detectors located on wall opposite dipoles in sections 8, 9, 0, 1 and 2 designed to avoid saturation on fast loss. Two types of detectors are used designated as SRLV's and SRVE's. SRLV's are standard scintillation-based loss monitors with the last 4 photo multiplier dynodes shorted to reduce gain, while the SRVE's are plastic scintillator detectors using vacuum photodiodes which won't saturate on extraction losses. Figure 8 shows a sample ΣSRVE signal (integrated) from a logbook showing a jump at extraction, which is proportional to the extraction loss. This system was calibrated by spilling (extraction septum magnets off) single beam pulse with known charge in the 1-turn extraction. The calibration constant has a factor of 2 or so uncertainty. With this system we measure a typical extraction loss of ~1 nC (~5-10% of total loss), which is roughly consistent with activation at the extraction septum region.

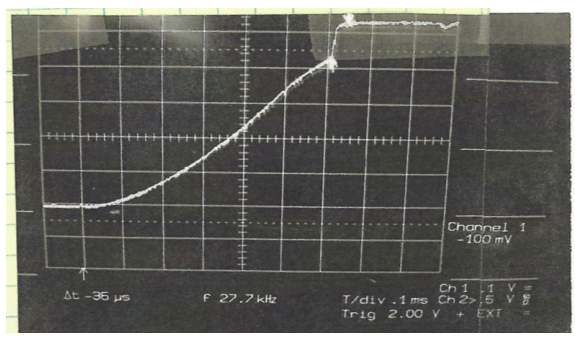

Figure 8: Example of extraction loss observed using an integrated ΣSRVE signal.

Space Charge Effect on Losses

The effect of space on beam losses was systematically measured on two occasions in 2001. Beam was accumulated for 1225 μs using the standard production injection offset and then the intensity was varied with jaws at the front of linac. All other accelerator parameters were held constant. The bunch width (aka pattern width PW) at injection was 280 ns (out of 358 ns revolution period) on 9/18/01 while on 10/17/01 it was 260 ns. The total fractional losses are plotted in Figure 9 as a function of accumulated charge per macropulse, Q. From this data we see that space charge does not significantly influence losses below 6 μC/pulse.

ISBN 978-3-95450-173-1

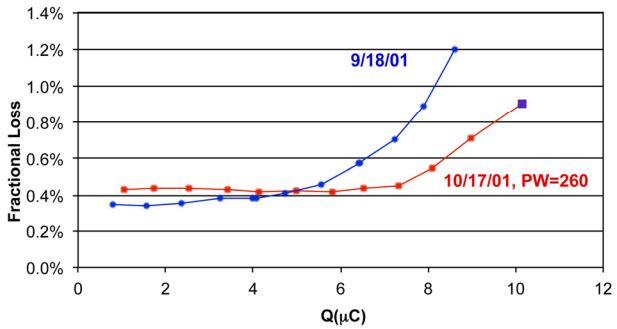

Figure 9: Fractional beam losses as a function of Q, the charge per macropulse.

MODELING LOSSES AT PSR

The ORBIT beam tracking code [2] with MAD8 matrices for the lattice model is used extensively at PSR to model beam dynamics effects including losses. It includes nuclear and Coulomb scattering in the foil, space charge effects, painting with programed bump magnets but production and stripping of H0(n) excited states are not included. We use numerous planar "black" apertures in various ring elements to obtain losses of proton beam. An example is shown in Figure 10 of the loss distribution from ORBIT modeling of the accumulation of a 5μC/macropulse production beam using the measured injection offset (2/3/14) and a measured injected beam phase space distribution (from 2010 experiment).

We use G4beamline code [3] to simulate the energy deposited in IR loss monitors with the local phase space distribution of proton loss from ORBIT as input. For an informative example we discuss the modeling of the energy deposited in IR's for the large (43 mm) horizontal bump in PSR Section 4.

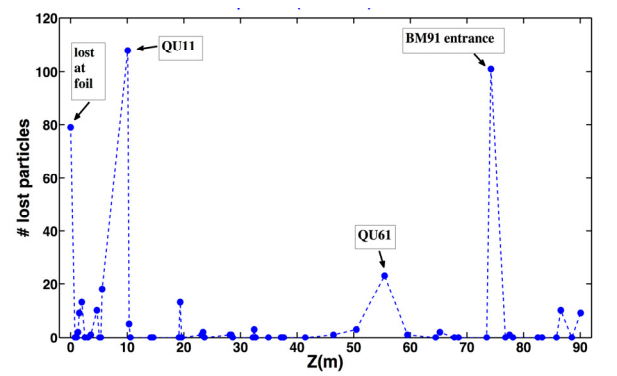

Figure 10: Lost particles as a function of distance Z from ORBIT modeling of production beam.

ORBIT modeling of the bump showed that 98 % of the loss was in one quad (SRQF41). The phase space distribution at the loss plane was extrapolated back to a point 0.5 m in front of the quad and used as input to G4Beamline of this region. This is depicted in the G4Beamline visualization of the area with secondary's from 10 lost protons in Figure 11.

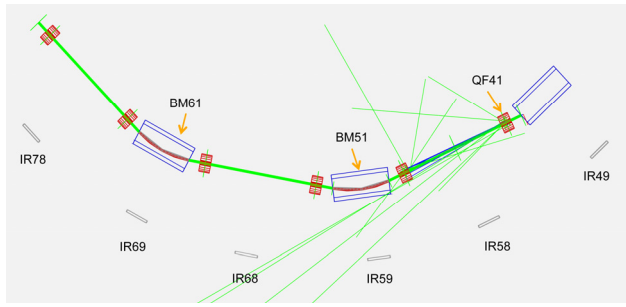

Figure 11: G4Beamline visualization plot of secondary particles from a spill in QF41 (positives: blue, neutrals: green, negatives: red).

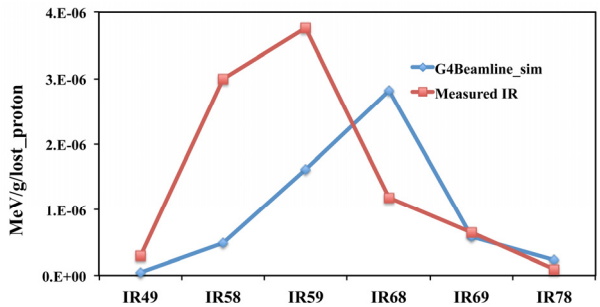

Figure 12: Energy deposited in IR's in region of SRQF41.

The energy deposited (MeV/g/lost_proton) in IR's from the G4Beamline simulation is plotted in Figure 12 and compared with the measured IR's signals converted to energy deposited (MeV/g/lost_proton) using the known calibration (5600 nC·Gy^{-1}) [14] of the ion chambers at PSR. For the summed energy of 6 IR's (IR49 through IR78), the simulation gave 5.78x10^{-6} MeV/g/lost_proton, which compares favorably to 8.98x10^{-6} MeV/g/lost_proton obtained from the measured IR signals, given the significant approximations in the material layout for the simulation.

CONCLUSIONS

Beam losses at high intensity proton accumulator rings such as PSR and SNS, in particular, PSR have been studied extensively for years and are now well understood. The observed fractional beam loss at PSR is typically 0.0025 ± 0.0005 for production beams after empirical optimization by operators. The breakdown by main components for PSR is: a) large angle Coulomb scattering = 0.0009, b) nuclear interactions plus elastic and inelastic scattering = 0.0010, c) H0(n) excited states = 0.0004, d) extraction loss ≤ 0.0002. It is worth noting that SNS has an order of magnitude lower loss but for a factor of 12 higher beam power.

The combination of ORBIT and G4Beamline codes are valuable tools for modeling both losses and the loss monitoring system (IRs) response. In addition to the

ISBN 978-3-95450-173-1

energy deposited in IR's, G4Beamline gives distribution of secondary particles striking down stream chamber walls, which is needed for modeling electron generation for the e-p instability. At PSR, beam loss from the e-p instability is just under control for production beams but is easily invoked especially during additional store time.

ACKNOWLEDGMENT

We gratefully acknowledge the contributions of the many people to the understanding of beam losses at PSR. D. Fitzgerald, M. Plum, A. Browman, L. Rybarcyk, R. McCrady, T. Spickermann, and M. Borden deserve special mention for their work. Finally, we acknowledge the skill and excellent cooperation of the LANSCE accelerator operating staff during our many experimental studies.

REFERENCES

[1] F. Christoph Iselin, The MAD Program 8.13, CERN-BE/ABP, (1994).
[2] Jeffrey A. Holmes et al., ICFA BD Newsletter, No. 30, p 100, (2003).
[3] T. Roberts, "G4Beamline User's Guide", http://www.muonsinternal.com/muons3/G4beamline
[4] George P. Lawrence, PAC 1987, p825 (1987).
[5] R. J. Macek et al, PAC 1993, p3739 (1993).
[6] R. Hutson and R. Macek, PAC 1993, p363 (1993).
[7] D. Fitzgerald et al., PAC 1999, p518 (1999).
[8] I. Sugai, HB2008, WGC08, p300, (2008).
[9] R. J. Macek et al., Proceedings of ECLOUD'04, CERN-2005-011, p63 (2005).
[10] R. Macek et al., Proceedings of ECLOUD10, OPR00, p1 (2010).
[11] J. D. Jackson, "Classical Electrodynamics", Wiley and Sons, (New York 1965).
[12] M. S. Gulley et al., Phys. Rev. A, **53**, 3201 (1996).
[13] "Rydberg States of Atoms and Molecules", Edited by R. F. Stebbings (CambridgeUniversity Press, Cambridge 1986).
[14] D. Brown et al., Nucl. Inst. and Meth. in Phys. Res. A **420** (1999) 494-506.

ISBN 978-3-95450-173-1